

# UniVerse: Unleashing the Scene Prior of Video Diffusion Models for Robust Radiance Field Reconstruction

Jin Cao<sup>1†</sup> Hongrui Wu<sup>2†</sup> Ziyong Feng<sup>3</sup> Hujun Bao<sup>1</sup> Xiaowei Zhou<sup>1</sup> Sida Peng<sup>1\*</sup>

<sup>1</sup>State Key Lab of CAD&CG, Zhejiang University <sup>2</sup>Tongji University <sup>3</sup>DeepGlint

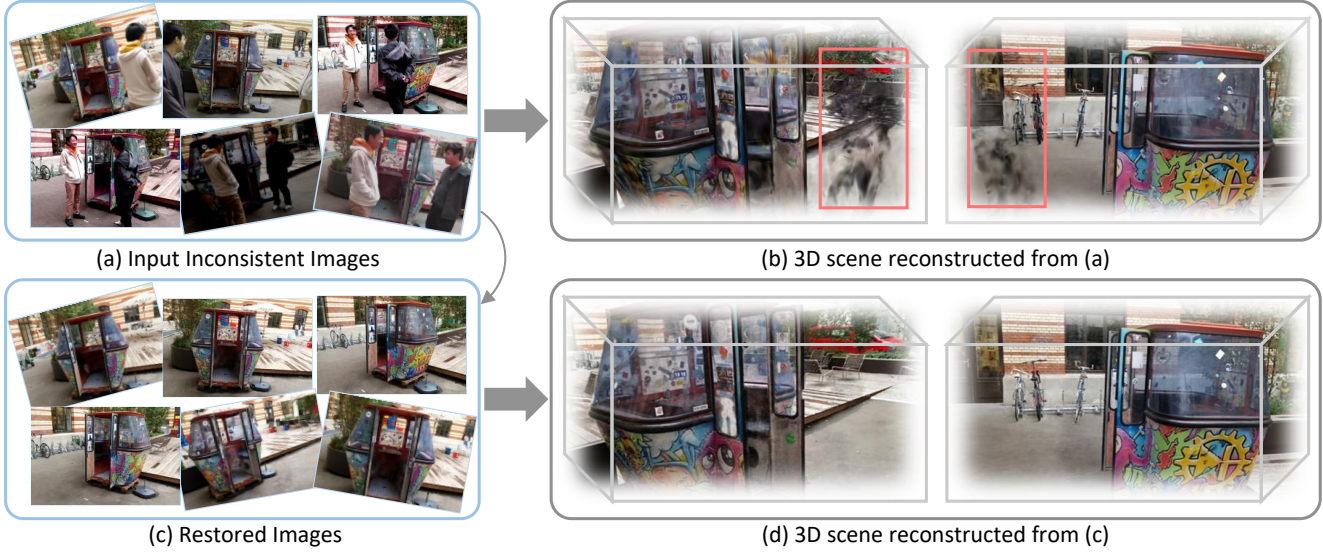


Figure 1. Given a set of inconsistent multi-view images with inconsistencies such as photometric variation or transient occlusions, as shown in (a), existing robust reconstruction methods often fail to produce a high-quality 3D scene with minimal artifacts and floaters when the views are not dense enough, as illustrated in (b). In contrast, our method first utilizes a Video Diffusion Model to restore all images into a consistent state in (c), and then reconstructs the 3D scene from these restored images, resulting in the high-quality 3D scene in (d).

## Abstract

This paper tackles the challenge of robust reconstruction, i.e., the task of reconstructing a 3D scene from a set of inconsistent multi-view images. Some recent works have attempted to simultaneously remove image inconsistencies and perform reconstruction by integrating image degradation modeling into neural 3D scene representations. However, these methods rely heavily on dense observations for robustly optimizing model parameters. To address this issue, we propose to decouple robust reconstruction into two subtasks: restoration and reconstruction, which naturally simplifies the optimization process. To this end, we introduce UniVerse, a unified framework for robust reconstruction based on a video diffusion model. Specifically, UniVerse first converts inconsistent images into initial videos,

then uses a specially designed video diffusion model to restore them into consistent images, and finally reconstructs the 3D scenes from these restored images. Compared with case-by-case per-view degradation modeling, the diffusion model learns a general scene prior from large-scale data, making it applicable to diverse image inconsistencies. Extensive experiments on both synthetic and real-world datasets demonstrate the strong generalization capability and superior performance of our method in robust reconstruction. Moreover, UniVerse can control the style of the reconstructed 3D scene. Project page: <https://jin-cao-tma.github.io/UniVerse.github.io/>.

## 1. Introduction

Novel view synthesis have long been a high-profile and complicated task in computer graphics, which plays a significant role in many applications like virtual reality (VR) and autonomous driving. Traditional approaches [48, 50]

† Co-first author. \*Corresponding author.

reconstruct 3D scenes based on the point cloud representation and multi-view stereo techniques. However, such methods generally suffer from low rendering quality, thus limiting their applications.

In recent years, differentiable rendering-based methods, such as Neural Radiance Fields (NeRF) [2, 3, 38, 40] and 3D Gaussian Splatting (3DGS) [7, 23, 28, 63], have made significant progress in rendering photorealistic novel views. However, these methods assume that all input images are static and captured under consistent conditions. In reality, images are frequently affected by illumination variations caused by changes in camera exposure or environmental lighting, content alterations due to dynamic objects, and motion blur resulting from camera shake. These inconsistencies violate the assumptions of the differentiable-rendering based methods, leading to significant performance degradation [35, 64].

To overcome this problem, previous methods propose learnable embeddings [10, 29, 35, 52] to additionally model the viewpoint-specific content for each image and jointly optimize it with the underlying 3D scene representation to minimize the rendering loss. When scene observations are sufficient, these methods can successfully recover the intrinsic scene structure from the inconsistent images. However, their performance tends to degrade significantly as the number of observations decreases. A plausible reason is that they introduce additional learnable parameters into the optimization process, making it more unstable, needing dense observations for optimization.

In this paper, we propose UniVerse, a video generative model for robust 3D reconstruction from inconsistent multi-view images. Our key idea is to exploit the strong consistent prior of video diffusion models [33, 67] to transform all inconsistent images to a consistent state before performing 3D reconstruction. Specifically, given a set of unstructured multi-view images, we first sort them to obtain a camera trajectory and insert blank images along this trajectory to transform images into a video. To better utilize observations, a multiple-input query transformer is proposed to aggregate information from all input images and generate a global semantic embedding, which is injected into the video diffusion model to help the video restoration. In contrast to previous methods that manually model the degradation in each image, the video diffusion model learns a general consistent scene prior from large-scale data, making it more robust in handling diverse inconsistencies.

We apply UniVerse to both synthetic and real-world challenging inconsistent image collections and demonstrate its ability to produce high-fidelity renderings with fewer artifacts and floaters, surpassing previous state-of-the-art methods in terms of PSNR, SSIM, and LPIPS. By selecting a style image, UniVerse can change the style of the generated videos to match that of the style image, thereby alter-

ing the style of the final reconstructed 3D scene. Even when the input images are very sparse and inconsistent (e.g., only 2 images with occlusions), UniVerse can still restore them into convincing consistent images, which can be applied to other downstream tasks such as generating new views [67] and performing further reconstruction. Overall, these results demonstrate the effectiveness of UniVerse and highlight the potential of decoupling robust reconstruction.

## 2. Related Works

### 2.1. Video Diffusion Models for 3D Reconstruction

The success of diffusion models has also spurred research in diffusion-based video generation [5, 5, 8, 27, 58], which are often fine-tuned from T2I models using extensive video datasets [1, 9, 62] and can generate consistent videos from text [5, 8, 27] or image inputs [5, 58]. Recent advancements [6, 8, 18, 54, 69, 72] further enhance text-to-video generation visual quality through extra temporal layers and curated datasets. The rapid developments of VDMs provoke significant interest in more controllable video generation, enabling controls like RGB images [5, 58, 59], depth [12, 60], trajectory [41, 65], and semantic maps [42]. Recently, some works further explore camera motion control for VDMs to generate controllable 3D-aware videos [5, 20, 39, 57]. Recently, CamCo [61] and CameraCtrl [21] introduced Plücker coordinates [49] in video diffusion models for camera motion control. ViewCrafter [67] and ReconX [33] further use explicit point clouds to achieve more precise 3D-aware camera control. These works achieve great success in generating consistent 3D-aware videos which can be directly used to reconstruct a 3D scene. Observing the strong consistent 3D prior of VDMs and noting that multi-view images are similar to frames extracted from a video captured by a camera trajectory, we take inconsistent multi-view images as conditions and generate a consistent video, and then extract them from the generated video with all images being consistent and static.

### 2.2. Robust 3D Reconstruction

Reconstructing a 3D scene from a set of 2D images is a long-standing problem in computer vision. Modern approaches, such as NeRF-based methods [15, 17, 40, 45, 66] and 3DGS-based methods [14, 23, 34, 68], have achieved great success and demonstrated expressive reconstruction quality. However, these methods all assume that the input images are captured in a static scene. Their performance declines significantly when reconstructing from unconstrained inconsistent photo collections. To address this challenging in-the-wild task, several attempts [10, 26, 29, 35, 36, 47, 64] have been made to handle appearance variation and transient occlusions. Other works [30, 31] focus on scenes with time-varying appearances, while methods [11, 25, 70] use

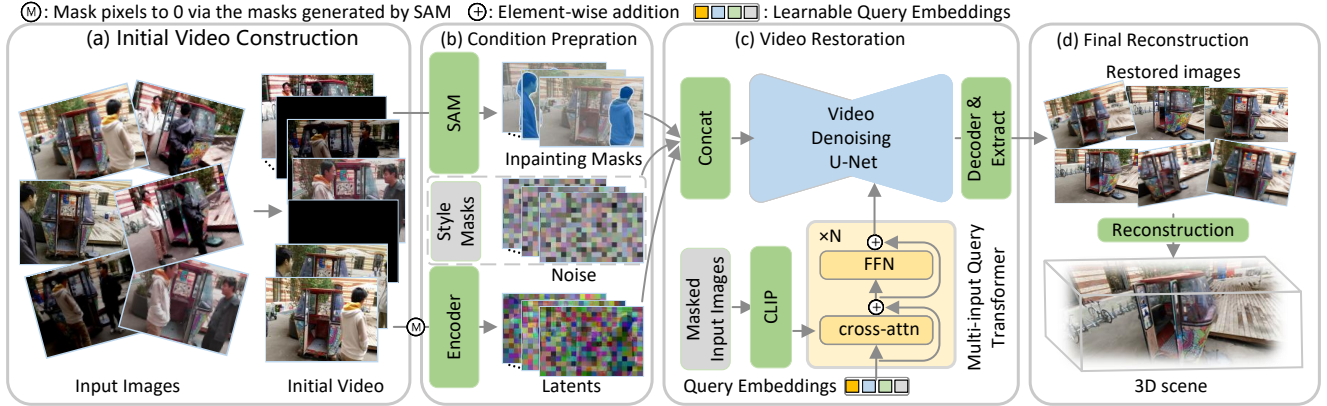


Figure 2. **The flowchart of UniVerse.** Given a set of inconsistent images, we first convert them into an initial video. We then use SAM [24] to identify transient occlusions and generate inpainting masks. These masks are used to set the occluded pixels in the initial video to zero. Next, we encode the video into latents using a VAE Encoder. After setting one image as the style image and assigning it style mask, we concatenate the style masks, inpainting masks, latents, and randomly sampled Gaussian noise along the channel dimension and feed them into the U-Net. For each masked input image, we obtain semantic embeddings using the CLIP image encoder and aggregate them via the Multi-input Query Transformer to form a global semantic embedding. This embedding guides the U-Net in the video generation process. Finally, the U-Net output is decoded by the VAE Decoder to produce the restored video, from which we extract the consistent images and reconstruct a high-quality 3D scene. If too many images for the VDM to restore at once, we iteratively restore them in batches as described.

physical rendering models for diverse lighting conditions. Nevertheless, these methods typically couple the process of restoration and reconstruction and directly perform reconstruction on the inconsistent multi-view images, which requires a large amount of training images to identify and remove all inconsistencies. What’s more, they typically use handcraft prior to manually model inconsistency in each image [55]. In contrast, our method emphasizes the effectiveness of restoration before reconstruction, decoupling the task and making it much easier. Meanwhile, the VDM we use learns a general consistent scene prior from large-scale data, thus can be more robust facing various inconsistencies. Recently, SimVS [53] utilized a multi-view diffusion model [16] to turn all images into a consistent state given an image as a reference. However, it retains all inconsistencies of the reference image, such as a moving passenger, thus can fail to reconstruct the static scene, while our method removes all inconsistencies in the images and aims to reconstruct the static scene.

### 3. Method

**Background.** 3D reconstruction aims to recover the 3D structure of a scene from multiple 2D images taken from different viewpoints. While traditional methods like structure-from-motion [48, 50] have been widely used, newer techniques such as NeRF [43] and 3DGS [23] leverage differentiable rendering. Given input images  $\{I_i\}_{i=1}^K$  and their corresponding poses  $\{P_i\}_{i=1}^K$ , differentiable rendering aims to find a parameterized function  $f_\theta$  that takes a camera pose as input and outputs the corresponding image.

The goal is to optimize the parameters  $\theta$  or the 3D representation to minimize the following loss function:

$$\theta = \arg \min_{\theta} \sum_{i=1}^K \text{Diff}(f_\theta(P_i), I_i). \quad (1)$$

Here,  $\text{Diff}(\cdot)$  is a differentiable function, such as MSE or L1 loss, used to measure the difference between two images. Once  $\theta$  is obtained, we can render novel views from the 3D scene for any new camera pose  $P$  using  $f_\theta(P)$ , thereby achieving 3D reconstruction. However, these approaches assume that the images  $\{I_i\}_{i=1}^K$  are consistent and static. If the assumption isn’t hold, the learning of  $f_\theta$  fails. To address this, UniVerse uses a VDM to restore all input images to be static and consistent. This ensures that the assumption for Eq. (1) is valid, helping  $f_\theta$  to easily learn the 3D scene.

**Overview.** Given  $K$  inconsistent multi-view images  $\{I_i\}_{i=1}^K, I_i \in \mathbb{R}^{3 \times H \times W}$ , our goal is to restore them into  $K$  consistent images. We treat the multi-view images as video frames from the same video. We first sort the images into ordered  $K$  images based on their camera poses, as described in in Sec. 3.1. Then we use a VDM to restore all these  $K$  images into a consistent state. Assuming the VDM can generate  $f$  frames at a time, we iteratively restore all images, processing  $N \leq f$  images per iteration. We select one of the first  $N$  images as the style image  $I_{sty}$ , and turn the first  $N$  images into an initial video as described in Sec. 3.1. For all frames in the initial video, we assign them inpainting masks to indicate where to be inpainted and style masks

to indicate which frame should be taken as the style reference via Segment Anything Model (SAM) [24]. Using the initial video, inpainting masks, and style masks as conditions, we use the VDM to generate a restored video with the same style as the style image, extracting the corresponding  $N$  consistent frames. We then remove the corresponding  $N$  images from the input unrestored  $K$  images since they are already restored, and add the last restored image to the unrestored images as the first image, and set it as style image for the next iteration. We update  $K$  to  $\max(K - (N - 1), 1)$  and repeat the process until  $K \leq 1$ , which means all images are restored. Finally, with all restored  $K$  images, we use 3D reconstruction methods like NeRFs [43] to reconstruct them and return a 3D representation. We show this process in Fig.2 and Alg. 1 in **Supp.**

### 3.1. Turning Multi-view Images into Videos

As discussed, UniVerse first converts the  $K$  input multi-view images into initial videos. These images are essentially captured by cameras at various poses around a single scene. Assuming all  $K$  poses  $\{P_i\}_{i=1}^K$  lie on a single camera trajectory, continuously sampling new poses (and thus new views) from this trajectory yields a video if the poses are sufficiently dense. This approach hinges on solving two key problems: (I) determining the trajectory and (II) sampling new poses from it. The detailed algorithm is provided in Sec. 7, Alg. 2 and Fig. 10 the **Supp.**

**Sorting Multi-view Images for Sparse Trajectory.** We use ThreadPose to sort the  $K$  input poses  $\{P_i\}_{i=1}^K$  into an ordered list. We initialize a double linked list with a randomly chosen pose and iteratively add the remaining poses based on their distances to the current head and tail of the list. The distance metric combines rotation and translation differences, weighted to ensure consistent scaling. Finally, we traverse the whole list to construct an ordered set of poses  $\{P'_i\}_{i=1}^K$ , which defines an implicit camera trajectory.

**Sample Implicit Dense Views from Trajectory** At each iteration, given  $N$  ordered poses  $\{P'_i\}_{i=1}^N$  and the corresponding  $N$  inconsistent images  $\{I'_i\}_{i=1}^N$ , our goal is to create an initial video of  $f$  frames that includes all  $N$  input images. We achieve this by sampling  $f - N$  new poses from the trajectory to generate new views. First, we compute the distances  $\{d_i\}_{i=1}^{N-1}$  between neighboring poses:

$$d_i = D_P(P'_i, P'_{i+1}), \quad i = 1, 2, \dots, N - 1. \quad (2)$$

Here,  $D_P(\cdot)$  is a function to compute the distance between two poses, which is defined in **Supp.** Next, we assign the number of new poses  $n_i$  to be inserted between each pair of neighboring poses  $P'_i$  and  $P'_{i+1}$ , proportional to the distance  $d_i$ . After assigning the number of poses, we aim to

sample new poses and new views. However, since the input images are inconsistent, it can be difficult to use methods like conditional VDM generation [21, 61], or building 3D structures like point clouds [67], to explicitly render a new view given an explicit camera pose. Considering VDM’s strong 3D prior and frame interpolation ability, we simply insert  $n_i$  zero frames into each  $I'_i, I'_{i+1}$  neighboring image pair and expect the VDM to inpaint these zero frames into new views. In this way, we turn  $N$  ordered images  $\{I'_i\}_{i=1}^N$  into an  $f$ -frame initial video with the first image  $I'_1$  and the last image  $I'_N$  as the first and last frames.

### 3.2. Conditional VDM for Initial Video Restoration

**Preliminary: Video Diffusion Models.** In diffusion-based video generation, Latent Diffusion Models (LDMs) [37] are often employed to reduce computational costs. In LDMs, video data  $x \in \mathbb{R}^{f \times 3 \times H \times W}$  is encoded into the latent space using a pre-trained VAE encoder frame-by-frame, expressed as  $z = \mathcal{E}(x)$ ,  $z \in \mathbb{R}^{f \times C \times h \times w}$ . The forward and reverse processes are then performed in the latent space. The final generated videos are obtained through the VAE decoder  $\hat{x} = \mathcal{D}(z)$ . In this work, we build our VDM based on an open-sourced Image-to-Video (I2V) diffusion model DynamiCrafter [58].

**Initial Video Restoration.** As shown in Fig. 2, at a certain iteration, given the input images and the corresponding initial video, inpainting masks, and style masks, we first use the VAE encoder to encode the initial video into latents and downsample both masks to match the shape of the latents. We then concatenate the latents, inpainting masks, style masks, and randomly sampled Gaussian noise along the channel dimension to form the image inputs.

To better leverage the I2V VDM’s ability to control video generation via text-aligned semantic embeddings [58], we extend the Query Transformer in [58] to a Multiple-input Query Transformer. Considering we have  $N$  input images per iteration, we pass them through the CLIP image encoder [44] to obtain  $N$  embeddings, which are then injected into the Multiple-input Query Transformer via cross-attention as the value and key. This yields a global semantic embedding to aid in generating 3D-aware videos.

With the image inputs and the embedding as conditional inputs, we use the VDM to generate restored latents and decode them using the VAE Decoder to produce the consistent restored video. Finally, we extract the corresponding  $N$  frames from the restored  $f$ -frame video as the restored images. We discard the other  $f - N$  new views, as they can be unreliable without 3D-consistency constraints.

**Training VDMs for Consistency.** As discussed, UniVerse aims to make input images consistent. The purpose of sampling dense views, as described in Sec. 3.1, is to trans-

form discrete images into a video to leverage the VDM’s prior, rather than generating new views. Directly training the VDM using MSE Loss is inappropriate because the simple MSE loss equally weights making the input  $N$  frames consistent and generating  $f - N$  new views. Given  $2 \leq N < f$ , we need to adjust the loss weights for each of the  $f$  frames to ensure the VDM focuses on making existing images consistent. To this end, we propose a consistency loss  $\mathcal{L}_{con}$  for VDM training. Specifically, assuming the initial video is  $\mathbf{v}^{ini} \in \mathbb{R}^{f \times 3 \times H \times W}$ , given the VDM’s estimated noise  $\epsilon_\theta$  and the ground truth noise  $\epsilon \in \mathbb{R}^{f \times C \times h \times w}$  during training, we first compute the MSE loss frame-by-frame to obtain the loss vector  $lv \in \mathbb{R}^f$ :

$$lv[i] = \|\epsilon_\theta[i] - \epsilon[i]\|_2^2, \quad \text{for } i = 1, 2, \dots, f, \quad (3)$$

where  $[i]$  denotes the  $i$ -th frame. We then adjust  $lv$  as follows:

$$lv[i] = lv[i] \times \begin{cases} \omega_c & \text{if } \mathbf{v}^{ini}[i] \text{ is an input image,} \\ \omega_n & \text{otherwise (i.e., } \mathbf{v}^{ro}[i] \text{ is a zero frame).} \end{cases} \quad (4)$$

The weights  $\omega_c$  and  $\omega_n$  are computed as:

$$\omega_c = \max\left(\frac{N}{f}, \lambda\right) / \frac{N}{f}, \quad (5)$$

$$\omega_n = \min\left(\frac{f - N}{N}, 1 - \lambda\right) / \frac{f - N}{f}. \quad (6)$$

This ensures that the ratio of the loss weights for making images consistent to generating new views is at least  $\lambda : (1 - \lambda)$ . In practice, we set  $\lambda$  to a large value like 0.98. Additionally, since our VDM takes initial video, inpainting/style masks as input, we need a special training data construction approach, which we discuss in Sec. 4.1.

## 4. Experiment

### 4.1. Implementation Details

**VDM Training Details:** We employ a progressive training strategy to fine-tune the VDM. Specifically, we fine-tune the  $576 \times 1024$  interpolation VDM from ViewCrafter [67]. In the first stage, we train the VDM at a resolution of  $320 \times 512$ , with the frame length  $f$  set to 25. The entire video denoising U-Net is fine-tuned for 14,520 iterations using a learning rate of  $5 \times 10^{-5}$  and a batch size of 8. In the second stage, we continue to fine-tune the video denoising U-Net at a resolution of  $576 \times 1024$  for high-resolution adaptation, with 12,000 iterations on a learning rate of  $1 \times 10^{-5}$  and a mini-batch size of 8. All training is conducted on 8 NVIDIA A100 GPUs.

**Training Data Construction:** Our VDM was trained on the DL3DV dataset [32]. Specifically, we first extract 25

frames from the video of DL3DV at a random FPS to simulate the varying levels of density and sparsity in real-world multi-view images. Then we randomly set  $n, 0 \leq n \leq 23$  of the 25 frames to zeros. Next, for each frame in the 25 frames, we randomly adjust their brightness, sharpness, hue, saturation, and simultaneously add Gaussian noise, motion blur, Gaussian blur, and occlusions to simulate inconsistencies. We use the VOC2007 dataset [13] to generate the occlusions and inpainting masks. In the masks, "1" indicates that this pixel needs to be inpainted, while "0" indicates the opposite. For zero frames, the inpainting masks are filled with "1". In this way, we generate a initial video and corresponding inpainting masks. Finally, we randomly choose a non-zero frame from the initial video as the style image and generate the style masks. Specifically, for the style frame, the mask is all "1", while for other frames, the mask is "0". We then adjust all frames in the original video to match the style of the style image to obtain the target video. In this way, we generate a training pair. In total, we generate 116,158 video pairs as training data.

**Inferencing Details:** During inference, we adopt the DDIM sampler [51] with classifier-free guidance [22]. We use SegNeXt [19] as the semantic segmentation model to identify transient occlusions in the input images, and then use SAM [24] to segment these occlusions and generate the inpainting masks. Assuming  $O$  is the minimum integer such that  $\frac{K-1}{O} < 25$ , we set the number of images processed at each iteration to  $N = \lfloor \frac{K-1}{O} \rfloor + 1$ . After all images are made consistent, we use ZipNeRF [4] with GLO [35] to reconstruct the 3D scene. All inference is conducted on a single NVIDIA A100 GPU.

### 4.2. Evaluation

We aim to evaluate the ability of UniVerse to alleviate the problem mentioned in the **Background** of Sec. 3, *i.e.* the problem of inconsistent images. We evaluate our method on both synthetic datasets and real-world datasets and compare it with the latest methods.

**Dataset:** For synthetic datasets, we utilize the NeRF llff dataset [43]. Since all images in this dataset are captured under static, consistent conditions, we randomly adjust their brightness, sharpness, hue, and saturation. We also randomly add Gaussian noise, motion blur, Gaussian blur, and occlusions to simulate inconsistencies. To stress test all methods, we limit the number of images for a single scene to 20-50. For real-world datasets, we use cell phone cameras to collect 7 real-world scenes for evaluation. During capture, in addition to the automatic adjustments by camera programs, we manually change local exposure and ISO settings, and apply random post-processing filters to each view. We show samples of our captured images in Fig. 5.

**Metrics and Compared Methods:** For quantitative comparison, we use PSNR, SSIM [56], and LPIPS [71] as



Figure 3. Visual results of novel view synthesis on synthetic datasets, with the corresponding depth map displayed in the bottom left corner.



Figure 4. Visual results of novel view synthesis on real datasets, with the corresponding depth map displayed in the bottom left corner.



Figure 5. Samples of our captured images.

metrics to assess the performance of our method. Meanwhile, we calculate a per-channel affine transformation to align the output color tints with the ground truth tints (Affine-aligned sRGB) [55]. We also present rendered images generated from the same pose as the input view for visual inspection. To demonstrate the superiority of our method, we compare it against the following meth-

Table 1. The quantitative results in novel view synthesis on synthetic datasets. The best and second-best results are highlighted.

	sRGB			Affine-aligned sRGB		
	PSNR $\uparrow$	SSIM $\uparrow$	LPIPS $\downarrow$	PSNR $\uparrow$	SSIM $\uparrow$	LPIPS $\downarrow$
ZipNeRF	11.52	0.2327	0.6930	14.53	0.3548	0.6297
ZipNeRF w/GLO	14.53	0.4667	0.4394	18.58	0.5297	0.4123
Bilarf	16.06	0.4814	0.4489	17.68	0.5062	0.4317
WildGaussians	13.75	0.3972	0.6430	15.45	0.4476	0.6244
Ours	18.09	0.5789	0.3015	20.12	0.5926	0.2979

ods: ZipNeRF [4], ZipNeRF W/GLO [35], Bilarf [55], and WildGaussians [26].

**Results:** We present the average quantitative results in Tab. 1 and Tab. 2, and the qualitative visual results in Fig. 3 and Fig. 4. Both tables show that UniVerse achieves the best metric values under both settings. Moreover, the figures demonstrate that our method provides the most visually

Table 2. The quantitative results in novel view synthesis on real-world datasets. The best and second-best results are highlighted.

	sRGB			Affine-aligned sRGB		
	PSNR $\uparrow$	SSIM $\uparrow$	LPIPS $\downarrow$	PSNR $\uparrow$	SSIM $\uparrow$	LPIPS $\downarrow$
ZipNeRF	13.31	0.5222	0.4310	16.38	0.5490	0.4328
ZipNeRF w/GLO	16.14	0.5668	0.3095	20.67	0.5907	0.3125
Bilarf	15.46	0.5459	0.3323	18.84	0.6055	0.3169
WildGaussians	15.05	0.4246	0.5046	17.39	0.5747	0.4493
Ours	19.65	0.6511	0.2532	22.91	0.6998	0.2132

pleasing results with fewer artifacts and floaters. In contrast, other compared methods often produce novel views with noticeable artifacts and a significant number of floaters due to unstable optimization and the lack of dense observations, thereby highlighting the superiority of our approach.

### 4.3. Abalation Study

#### The Effect of the Design of Turning Images into Videos:

As discussed, transforming multi-view images into videos is crucial for unleashing the consistent 3D prior of VDMs. To validate this, we tested the following settings for image restoration and reconstruction: (a) Directly stacking unordered images as the initial video. (b) Sorting images using ThreadPose and stacking them as the initial video. (c) Inserting zero frames (implicit views) into unordered images to form the initial video. (d) Inserting zero frames into ordered images, as described in Sec. 3.1. The results in Tab. 3 show that only our design fully exploits the 3D prior of VDMs, demonstrating its rationality.

Table 3. Results on novel view synthesis with different image to video settings.

Setting	<i>ThreadPose</i>	<i>zero frames</i>	PSNR	SSIM
(a) ( <i>directly stack</i> )	✗	✗	15.32	0.4598
(b) ( <i>w/ ThreadPose</i> )	✓	✗	17.29	0.5876
(c) ( <i>w/ zero frames</i> )	✗	✓	18.25	0.6067
(d) ( <i>ours</i> )	✓	✓	20.71	0.7708

**The Effect of our VDM Design:** We introduce four new designs for VDMs in this work: the Multi-input Query Transformer (MiQT), style mask, inpainting mask, and consistent loss. We validate each design as follows:

(1) **Multi-input Query Transformer (MiQT):** To assess MiQT’s impact, we retrained a model using a single-input QT and compared its robust reconstruction performance with ours. The results in Tab. 4 show MiQT’s superiority over QT. This highlights the importance of global semantic information in leveraging VDMs’ prior, thereby justifying our design.

(2) **Inpainting Mask:** We retrained a VDM without inpainting masks, forcing it to decide which pixels to inpaint. Using a subset of the NeRF-on-the-go dataset [46] contain-

Table 4. Results on novel view synthesis with different Query Transformer (QT) settings.

Setting	PSNR	SSIM	LPIPS	Setting	PSNR	SSIM	LPIPS
QT	16.80	0.4157	0.5015	MiQT	17.42	0.4511	0.4549

ing only occlusions as inconsistencies, we found that the VDM failed to inpaint all masked pixels (Fig. 8). Thus, inpainting masks are essential for UniVerse.

(3) **Style Mask:** Figure 9 compares results with and without the style mask. Without it, output image tone is uncontrollable despite consistent input tones. Style masks are thus crucial for controlling image appearance and reconstructed 3D scene style.

(4) **Consistent Loss:** As elaborated in Sec. 3.2, employing the Consistent Loss is pivotal for directing the VDM to prioritize image consistency. The comparative training outcomes presented in Tab. 5 underscore the superior performance of the Consistent Loss over the regular MSE. This superiority indicates that the Consistent Loss effectively enables the VDM to more adeptly eliminate inconsistencies, thereby substantiating the efficacy of our design approach.

Table 5. Results on novel view synthesis with different training loss function settings.

Setting	PSNR	SSIM	LPIPS	Setting	PSNR	SSIM	LPIPS
MSE	16.19	0.3788	0.5340	Consistent	17.42	0.4511	0.4549

### 4.4. Further Applications of UniVerse

**Controlling the Style of Reconstructed 3D Scene:** The style of the restored images, and consequently the reconstructed 3D scenes, is determined by the style image. By changing the style image, we can alter the style of the entire reconstructed 3D scene, as shown in Fig. 6.

**Robust Reconstruction on Sparse Images:** UniVerse focuses on making images consistent rather than generating new views. Thus, even after restoring very sparse input images to a consistent state, reconstruction may still fail due to insufficient views. This issue can be easily resolved by using a generative novel view synthesis model like ViewCrafter [67]. As shown in Fig. 7, given 2 inconsistent input images, ViewCrafter [67] synthesizes distorted novel views with strange occlusions. After the images are restored via UniVerse, the novel views synthesized by ViewCrafter become consistent. In other words, as a restoration model, UniVerse can serve as a pre-processor for other models, enabling robust reconstruction.

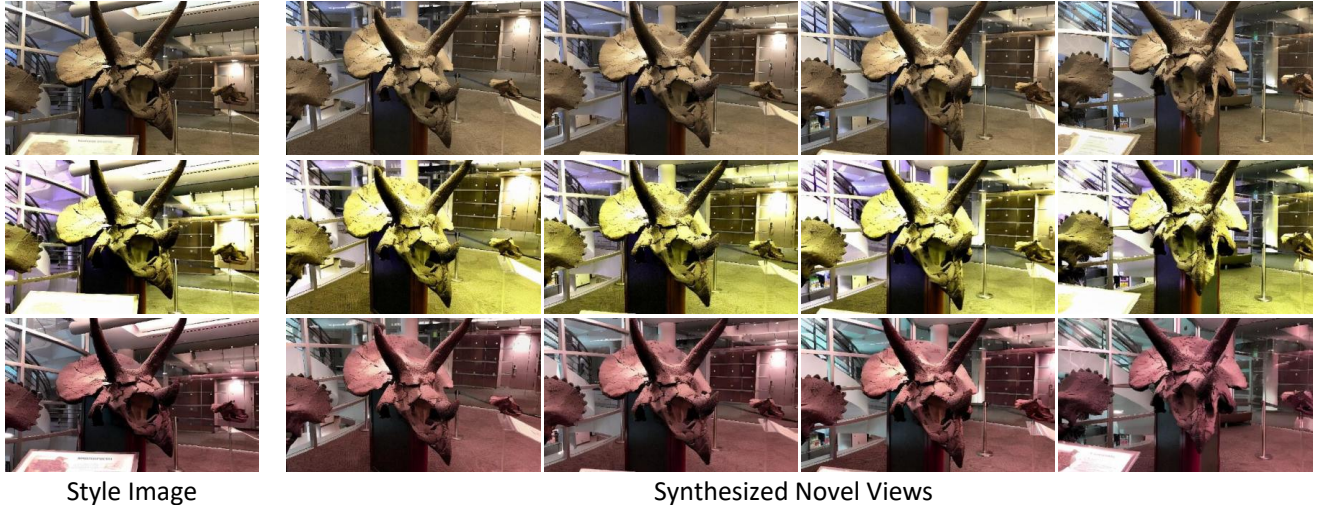


Figure 6. Controlling the style of reconstructed 3D scene by switching style image.



Figure 7. Novel views synthesized via ViewCrafter [67]. **First line:** ViewCrafter synthesizes inconsistent and distorted views from inconsistent images. **Second line:** After the images are restored by UniVerse, the generated views become consistent.



Figure 8. Visualization of results w/o and w/ inpainting masks.



Figure 9. Visualization of results w/o and w/ style masks.

## 5. Conclusion & Limitation

This paper proposes UniVerse, a unified robust reconstruction framework that converts inconsistent multi-view im-

ages into initial videos and leverages Video Diffusion Models to restore them into consistent images. By decoupling robust reconstruction into two subtasks (*i.e.* restoration and reconstruction), UniVerse overcomes the limitations of existing approaches that require very dense observations to reconstruct inconsistent images, achieving state-of-the-art performance on both synthetic and real-world datasets. Moreover, we explore UniVerse’s ability to control the style of the reconstructed 3D scene by switching the reference image and its potential for reconstructing very sparse inconsistent observations by applying novel view generation models after restoration. We believe our work offers new insights of decoupling robust reconstruction and restoring images using models with 3D priors to the community.

**Limitations:** UniVerse requires synthesizing videos with inconsistencies as training data to fine-tune the VDM for adaptation to a restoration model. While some inconsistencies, like lighting, may be hard to synthesize, [53] have shown tremendous promise for inconsistency synthesis via generative models.

## 6. Acknowledgment

This work was partially supported by the National Key R&D Program of China (No. 2024YFB2809102), NSFC (No. 62402427, NO. U24B20154), Zhejiang Provincial Natural Science Foundation of China (No. LR25F020003), DeepGlint, Zhejiang University Education Foundation Qizhen Scholar Foundation, and Information Technology Center and State Key Lab of CAD&CG, Zhejiang University.

## References

- [1] Max Bain, Arsha Nagrani, Gül Varol, and Andrew Zisserman. Frozen in time: A joint video and image encoder for end-to-end retrieval. In *ICCV*, 2021. 2
- [2] Jonathan T Barron, Ben Mildenhall, Matthew Tancik, Peter Hedman, Ricardo Martin-Brualla, and Pratul P Srinivasan. Mip-nerf: A multiscale representation for anti-aliasing neural radiance fields. In *ICCV*, 2021. 2
- [3] Jonathan T Barron, Ben Mildenhall, Dor Verbin, Pratul P Srinivasan, and Peter Hedman. Mip-nerf 360: Unbounded anti-aliased neural radiance fields. In *CVPR*, 2022. 2
- [4] Jonathan T. Barron, Ben Mildenhall, Dor Verbin, Pratul P. Srinivasan, and Peter Hedman. Zip-nerf: Anti-aliased grid-based neural radiance fields. *ICCV*, 2023. 5, 6
- [5] Andreas Blattmann, Tim Dockhorn, Sumith Kulal, Daniel Mendelevitch, Maciej Kilian, Dominik Lorenz, Yam Levi, Zion English, Vikram Voleti, Adam Letts, et al. Stable video diffusion: Scaling latent video diffusion models to large datasets. *arXiv preprint arXiv:2311.15127*, 2023. 2
- [6] Andreas Blattmann, Robin Rombach, Huan Ling, Tim Dockhorn, Seung Wook Kim, Sanja Fidler, and Karsten Kreis. Align your latents: High-resolution video synthesis with latent diffusion models. In *CVPR*, 2023. 2
- [7] Danpeng Chen, Hai Li, Weicai Ye, Yifan Wang, Weijian Xie, Shangjin Zhai, Nan Wang, Haomin Liu, Hujun Bao, and Guofeng Zhang. Pgsr: Planar-based gaussian splatting for efficient and high-fidelity surface reconstruction. *arXiv preprint arXiv:2406.06521*, 2024. 2
- [8] Haoxin Chen, Menghan Xia, Yingqing He, Yong Zhang, Xiaodong Cun, Shaoshu Yang, Jinbo Xing, Yaofang Liu, Qifeng Chen, Xintao Wang, et al. Videocrafter1: Open diffusion models for high-quality video generation. *arXiv preprint arXiv:2310.19512*, 2023. 2
- [9] Tsai-Shien Chen, Aliaksandr Siarohin, Willi Menapace, Ekaterina Deyneka, Hsiang-wei Chao, Byung Eun Jeon, Yuwei Fang, Hsin-Ying Lee, Jian Ren, Ming-Hsuan Yang, et al. Panda-70m: Captioning 70m videos with multiple cross-modality teachers. In *CVPR*, 2024. 2
- [10] Xingyu Chen, Qi Zhang, Xiaoyu Li, Yue Chen, Ying Feng, Xuan Wang, and Jue Wang. Hallucinated neural radiance fields in the wild. In *Proceedings of the IEEE/CVF Conference on Computer Vision and Pattern Recognition*, pages 12943–12952, 2022. 2
- [11] Andreas Engelhardt, Amit Raj, Mark Boss, Yunzhi Zhang, Abhishek Kar, Yuanzhen Li, Deqing Sun, Ricardo Martin Brualla, Jonathan T Barron, Hendrik Lensch, et al. Shinobi: Shape and illumination using neural object decomposition via brdf optimization in-the-wild. In *Proceedings of the IEEE/CVF Conference on Computer Vision and Pattern Recognition*, pages 19636–19646, 2024. 2
- [12] Patrick Esser, Johnathan Chiu, Parmida Atighehchian, Jonathan Granskog, and Anastasis Germanidis. Structure and content-guided video synthesis with diffusion models. In *ICCV*, 2023. 2
- [13] M. Everingham, L. Van Gool, C. K. I. Williams, J. Winn, and A. Zisserman. The PASCAL Visual Object Classes Challenge 2007 (VOC2007) Results. <http://www.pascal-network.org/challenges/VOC/voc2007/workshop/index.html>. 5
- [14] Zhiwen Fan, Kevin Wang, Kairun Wen, Zehao Zhu, De-jia Xu, and Zhangyang Wang. Lightgaussian: Unbounded 3d gaussian compression with 15x reduction and 200+ fps. *arXiv preprint arXiv:2311.17245*, 2023. 2
- [15] Sara Fridovich-Keil, Alex Yu, Matthew Tancik, Qinhong Chen, Benjamin Recht, and Angjoo Kanazawa. Plenoxels: Radiance fields without neural networks. In *Proceedings of the IEEE/CVF Conference on Computer Vision and Pattern Recognition*, pages 5501–5510, 2022. 2
- [16] Ruiqi Gao, Aleksander Holynski, Philipp Henzler, Arthur Brussee, Ricardo Martin-Brualla, Pratul Srinivasan, Jonathan T Barron, and Ben Poole. Cat3d: Create anything in 3d with multi-view diffusion models. *arXiv preprint arXiv:2405.10314*, 2024. 3
- [17] Stephan J Garbin, Marek Kowalski, Matthew Johnson, Jamie Shotton, and Julien Valentin. Fastnerf: High-fidelity neural rendering at 200fps. In *ICCV*, 2021. 2
- [18] Songwei Ge, Seungjun Nah, Guilin Liu, Tyler Poon, Andrew Tao, Bryan Catanzaro, David Jacobs, Jia-Bin Huang, Ming-Yu Liu, and Yogesh Balaji. Preserve your own correlation: A noise prior for video diffusion models. In *ICCV*, 2023. 2
- [19] Meng-Hao Guo, Cheng-Ze Lu, Qibin Hou, Zhengning Liu, Ming-Ming Cheng, and Shi-min Hu. Segnext: Rethinking convolutional attention design for semantic segmentation. In *Advances in Neural Information Processing Systems*, pages 1140–1156. Curran Associates, Inc., 2022. 5
- [20] Yuwei Guo, Ceyuan Yang, Anyi Rao, Yaohui Wang, Yu Qiao, Dahua Lin, and Bo Dai. Animatediff: Animate your personalized text-to-image diffusion models without specific tuning. *arXiv preprint arXiv:2307.04725*, 2023. 2
- [21] Hao He, Yinghao Xu, Yuwei Guo, Gordon Wetzstein, Bo Dai, Hongsheng Li, and Ceyuan Yang. Cameractrl: Enabling camera control for text-to-video generation. *arXiv preprint arXiv:2404.02101*, 2024. 2, 4
- [22] Jonathan Ho and Tim Salimans. Classifier-free diffusion guidance. *arXiv preprint arXiv:2207.12598*, 2022. 5
- [23] Bernhard Kerbl, Georgios Kopanas, Thomas Leimkühler, and George Drettakis. 3d gaussian splatting for real-time radiance field rendering. *ACM Transactions on Graphics*, 42(4), 2023. 2, 3
- [24] Alexander Kirillov, Eric Mintun, Nikhila Ravi, Hanzi Mao, Chloe Rolland, Laura Gustafson, Tete Xiao, Spencer Whitehead, Alexander C. Berg, Wan-Yen Lo, Piotr Dollár, and

- Ross Girshick. Segment anything. *arXiv:2304.02643*, 2023. 3, 4, 5
- [25] Zhengfei Kuang, Kyle Olszewski, Menglei Chai, Zeng Huang, Panos Achlioptas, and Sergey Tulyakov. Neroc: Neural rendering of objects from online image collections. *ACM Transactions on Graphics (TOG)*, 41(4):1–12, 2022. 2
- [26] Jonas Kulhanek, Songyou Peng, Zuzana Kukelova, Marc Pollefeys, and Torsten Sattler. Wildgaussians: 3d gaussian splatting in the wild. *NeurIPS*, 2024. 2, 6
- [27] PKU-Yuan Lab and Tuzhan AI etc. Open-sora-plan. <https://github.com/PKU-YuanGroup/Open-Sora-Plan>, 2024. 2
- [28] Joo Chan Lee, Daniel Rho, Xiangyu Sun, Jong Hwan Ko, and Eunbyung Park. Compact 3d gaussian representation for radiance field. In *Proceedings of the IEEE/CVF Conference on Computer Vision and Pattern Recognition (CVPR)*, pages 21719–21728, 2024. 2
- [29] Peihao Li, Shaohui Wang, Chen Yang, Bingbing Liu, Weichao Qiu, and Haoqian Wang. Nerf-ms: Neural radiance fields with multi-sequence. In *Proceedings of the IEEE/CVF International Conference on Computer Vision*, pages 18591–18600, 2023. 2
- [30] Zhengqi Li, Wenqi Xian, Abe Davis, and Noah Snavely. Crowdsampling the plenoptic function. In *Computer Vision—ECCV 2020: 16th European Conference, Glasgow, UK, August 23–28, 2020, Proceedings, Part I 16*, pages 178–196. Springer, 2020. 2
- [31] Haotong Lin, Qianqian Wang, Ruojin Cai, Sida Peng, Hadar Averbuch-Elor, Xiaowei Zhou, and Noah Snavely. Neural scene chronology. In *Proceedings of the IEEE/CVF Conference on Computer Vision and Pattern Recognition*, pages 20752–20761, 2023. 2
- [32] Lu Ling, Yichen Sheng, Zhi Tu, Wentian Zhao, Cheng Xin, Kun Wan, Lantao Yu, Qianyu Guo, Zixun Yu, Yawen Lu, et al. D3dv-10k: A large-scale scene dataset for deep learning-based 3d vision. In *CVPR*, 2024. 5
- [33] Fangfu Liu, Wenqiang Sun, Hanyang Wang, Yikai Wang, Haowen Sun, Junliang Ye, Jun Zhang, and Yueqi Duan. Reconx: Reconstruct any scene from sparse views with video diffusion model, 2024. 2
- [34] Tao Lu, Mulin Yu, Linning Xu, Yuanbo Xiangli, Limin Wang, Dahua Lin, and Bo Dai. Scaffold-gs: Structured 3d gaussians for view-adaptive rendering. *arXiv preprint arXiv:2312.00109*, 2023. 2
- [35] Ricardo Martin-Brualla, Noha Radwan, Mehdi SM Sajjadi, Jonathan T Barron, Alexey Dosovitskiy, and Daniel Duckworth. Nerf in the wild: Neural radiance fields for unconstrained photo collections. In *Proceedings of the IEEE/CVF Conference on Computer Vision and Pattern Recognition*, pages 7210–7219, 2021. 2, 5, 6
- [36] Moustafa Meshry, Dan B Goldman, Sameh Khamis, Hugues Hoppe, Rohit Pandey, Noah Snavely, and Ricardo Martin-Brualla. Neural rerendering in the wild. In *Proceedings of the IEEE/CVF Conference on Computer Vision and Pattern Recognition*, pages 6878–6887, 2019. 2
- [37] Gal Metzer, Elad Richardson, Or Patashnik, Raja Giryes, and Daniel Cohen-Or. Latent-nerf for shape-guided generation of 3d shapes and textures. In *CVPR*, 2023. 4, 3
- [38] Ben Mildenhall, Pratul P Srinivasan, Matthew Tancik, Jonathan T Barron, Ravi Ramamoorthi, and Ren Ng. Nerf: Representing scenes as neural radiance fields for view synthesis. *Communications of the ACM*, 65(1):99–106, 2021. 2
- [39] Norman Müller, Katja Schwarz, Barbara Rössle, Lorenzo Porzi, Samuel Rota Bulò, Matthias Nießner, and Peter Kotschieder. Multidiff: Consistent novel view synthesis from a single image. In *CVPR*, 2024. 2
- [40] Thomas Müller, Alex Evans, Christoph Schied, and Alexander Keller. Instant neural graphics primitives with a multiresolution hash encoding. *ACM Transactions on Graphics (ToG)*, 41(4):1–15, 2022. 2
- [41] Muyao Niu, Xiaodong Cun, Xintao Wang, Yong Zhang, Ying Shan, and Yinqiang Zheng. Mofa-video: Controllable image animation via generative motion field adaptations in frozen image-to-video diffusion model. *arXiv preprint arXiv:2405.20222*, 2024. 2
- [42] Elia Peruzzo, Vidit Goel, Deji Xu, Xingqian Xu, Yifan Jiang, Zhangyang Wang, Humphrey Shi, and Nicu Sebe. Vase: Object-centric appearance and shape manipulation of real videos. *arXiv preprint arXiv:2401.02473*, 2024. 2
- [43] Chen Quei-An. Nerf pl: a pytorch-lightning implementation of nerf. URL [https://github.com/kweal23/nerf\\_pl](https://github.com/kweal23/nerf_pl), 5, 2020. 3, 4, 5
- [44] Alec Radford, Jong Wook Kim, Chris Hallacy, Aditya Ramesh, Gabriel Goh, Sandhini Agarwal, Girish Sastry, Amanda Askell, Pamela Mishkin, Jack Clark, et al. Learning transferable visual models from natural language supervision. In *ICML*, 2021. 4
- [45] Christian Reiser, Songyou Peng, Yiyi Liao, and Andreas Geiger. Kilonerf: Speeding up neural radiance fields with thousands of tiny mlps. In *ICCV*, 2021. 2
- [46] Weining Ren, Zihan Zhu, Boyang Sun, Jiaqi Chen, Marc Pollefeys, and Songyou Peng. Nerf on-the-go: Exploiting uncertainty for distractor-free nerfs in the wild. In *IEEE/CVF Conference on Computer Vision and Pattern Recognition (CVPR)*, 2024. 7
- [47] Viktor Rudnev, Mohamed Elgharib, William Smith, Lingjie Liu, Vladislav Golyanik, and Christian Theobalt. Nerf for outdoor scene relighting. In *European Conference on Computer Vision*, pages 615–631. Springer, 2022. 2
- [48] Johannes L Schonberger and Jan-Michael Frahm. Structure-from-motion revisited. In *Proceedings of the IEEE conference on computer vision and pattern recognition*, pages 4104–4113, 2016. 1, 3
- [49] Vincent Sitzmann, Semon Rezchikov, Bill Freeman, Josh Tenenbaum, and Fredo Durand. Light field networks: Neural scene representations with single-evaluation rendering. In *NeurIPS*, 2021. 2
- [50] Noah Snavely, Steven M. Seitz, and Richard Szeliski. Modeling the world from internet photo collections. *International Journal of Computer Vision*, 80:189–210, 2008. 1, 3
- [51] Jiaming Song, Chenlin Meng, and Stefano Ermon. Denoising diffusion implicit models. In *ICLR*, 2021. 5
- [52] Matthew Tancik, Vincent Casser, Xinchen Yan, Sabeek Pradhan, Ben Mildenhall, Pratul P Srinivasan, Jonathan T Barron,

- and Henrik Kretzschmar. Block-nerf: Scalable large scene neural view synthesis. In *CVPR*, 2022. 2
- [53] Alex Trevithick, Roni Paiss, Philipp Henzler, Dor Verbin, Rundi Wu, Hadi Alzayer, Ruiqi Gao, Ben Poole, Jonathan T. Barron, Aleksander Holynski, Ravi Ramamoorthi, and Pratul P. Srinivasan. Simvs: Simulating world inconsistencies for robust view synthesis, 2024. 3, 8
- [54] Yaohui Wang, Xinyuan Chen, Xin Ma, Shangchen Zhou, Ziqi Huang, Yi Wang, Ceyuan Yang, Yinan He, Jiashuo Yu, Peiqing Yang, et al. Lavie: High-quality video generation with cascaded latent diffusion models. *arXiv preprint arXiv:2309.15103*, 2023. 2
- [55] Yuehao Wang, Chaoyi Wang, Bingchen Gong, and Tianfan Xue. Bilateral guided radiance field processing. *ACM Transactions on Graphics (TOG)*, 43(4):1–13, 2024. 3, 6
- [56] Zhou Wang, Alan C Bovik, Hamid R Sheikh, and Eero P Simoncelli. Image quality assessment: from error visibility to structural similarity. *IEEE TIP*, 13(4):600–612, 2004. 5
- [57] Zhouxia Wang, Ziyang Yuan, Xintao Wang, Tianshui Chen, Menghan Xia, Ping Luo, and Ying Shan. Motionctrl: A unified and flexible motion controller for video generation. In *SIGGRAPH Conference*, 2024. 2
- [58] Jinbo Xing, Menghan Xia, Yong Zhang, Haoxin Chen, Xintao Wang, Tien-Tsin Wong, and Ying Shan. Dynamicrafter: Animating open-domain images with video diffusion priors. *arXiv preprint arXiv:2310.12190*, 2023. 2, 4
- [59] Jinbo Xing, Hanyuan Liu, Menghan Xia, Yong Zhang, Xintao Wang, Ying Shan, and Tien-Tsin Wong. Toonrafter: Generative cartoon interpolation. *arXiv preprint arXiv:2405.17933*, 2024. 2
- [60] Jinbo Xing, Menghan Xia, Yuxin Liu, Yuechen Zhang, Yong Zhang, Yingqing He, Hanyuan Liu, Haoxin Chen, Xiaodong Cun, Xintao Wang, et al. Make-your-video: Customized video generation using textual and structural guidance. *IEEE TVCG*, 2024. 2
- [61] Dejjia Xu, Weili Nie, Chao Liu, Sifei Liu, Jan Kautz, Zhangyang Wang, and Arash Vahdat. Camco: Camera-controllable 3d-consistent image-to-video generation. *arXiv preprint arXiv:2406.02509*, 2024. 2, 4
- [62] Hongwei Xue, Tiankai Hang, Yanhong Zeng, Yuchong Sun, Bei Liu, Huan Yang, Jianlong Fu, and Baining Guo. Advancing high-resolution video-language representation with large-scale video transcriptions. In *CVPR*, 2022. 2
- [63] Yunzhi Yan, Haotong Lin, Chenxu Zhou, Weijie Wang, Haiyang Sun, Kun Zhan, Xianpeng Lang, Xiaowei Zhou, and Sida Peng. Street gaussians: Modeling dynamic urban scenes with gaussian splatting. In *ECCV*, 2024. 2
- [64] Yifan Yang, Shuhai Zhang, Zixiong Huang, Yubing Zhang, and Mingkui Tan. Cross-ray neural radiance fields for novel-view synthesis from unconstrained image collections. In *Proceedings of the IEEE/CVF International Conference on Computer Vision*, pages 15901–15911, 2023. 2
- [65] Shengming Yin, Chenfei Wu, Jian Liang, Jie Shi, Houqiang Li, Gong Ming, and Nan Duan. Dragnuwa: Fine-grained control in video generation by integrating text, image, and trajectory. *arXiv preprint arXiv:2308.08089*, 2023. 2
- [66] Alex Yu, Ruilong Li, Matthew Tancik, Hao Li, Ren Ng, and Angjoo Kanazawa. Plenotrees for real-time rendering of neural radiance fields. In *ICCV*, 2021. 2
- [67] Wangbo Yu, Jinbo Xing, Li Yuan, Wenbo Hu, Xiaoyu Li, Zhipeng Huang, Xiangjun Gao, Tien-Tsin Wong, Ying Shan, and Yonghong Tian. Viewcrafter: Taming video diffusion models for high-fidelity novel view synthesis. *arXiv preprint arXiv:2409.02048*, 2024. 2, 4, 5, 7, 8, 3
- [68] Zehao Yu, Anpei Chen, Binbin Huang, Torsten Sattler, and Andreas Geiger. Mip-splatting: Alias-free 3d gaussian splatting. *arXiv preprint arXiv:2311.16493*, 2023. 2
- [69] David Junhao Zhang, Jay Zhangjie Wu, Jia-Wei Liu, Rui Zhao, Lingmin Ran, Yuchao Gu, Difei Gao, and Mike Zheng Shou. Show-1: Marrying pixel and latent diffusion models for text-to-video generation. *arXiv preprint arXiv:2309.15818*, 2023. 2
- [70] Jason Zhang, Gengshan Yang, Shubham Tulsiani, and Deva Ramanan. Ners: Neural reflectance surfaces for sparse-view 3d reconstruction in the wild. *Advances in Neural Information Processing Systems*, 34:29835–29847, 2021. 2
- [71] Richard Zhang, Phillip Isola, Alexei A Efros, Eli Shechtman, and Oliver Wang. The unreasonable effectiveness of deep features as a perceptual metric. In *CVPR*, 2018. 5
- [72] Daquan Zhou, Weimin Wang, Hanshu Yan, Weiwei Lv, Yizhe Zhu, and Jiashi Feng. Magicvideo: Efficient video generation with latent diffusion models. *arXiv preprint arXiv:2211.11018*, 2022. 2

# UniVerse: Unleashing the Scene Prior of Video Diffusion Models for Robust Radiance Field Reconstruction

## Supplementary Material

### 7. More Details for Method

#### 7.1. Sorting Images for Sparse Trajectory.

Starting with  $K$  poses  $\{P_i\}_{i=1}^K$ , we initialize a double linked list  $\{P_i^l\}_{i=1}^L$  with a randomly chosen pose  $P_{\text{init}} \in \{P_i\}_{i=1}^K$ , where  $L$  is the length of the list. At each iteration, for any pose  $P_c \in \{P_i\}_{i=1}^K \setminus \{P_i^l\}_{i=1}^L$ , we calculate its distance with the list  $D_{PL}$  as follows:

$$D_{PL}(P_c, \{P_i^l\}_{i=1}^L) = \min\{D_P(P_c, P_{\text{head}}^l), D_P(P_c, P_{\text{tail}}^l)\}. \quad (7)$$

Here,  $P_{\text{head}}^l$  and  $P_{\text{tail}}^l$  are the head and tail of the current list, i.e.,  $P_1^l$  and  $P_L^l$ . The distance between poses  $D_P$  is defined as:

$$D_P(P_a, P_b) = \frac{\omega_r}{s_R} \cdot D_R(R_a, R_b) + \frac{1 - \omega_r}{s_T} \cdot D_T(T_a, T_b). \quad (8)$$

Here,  $R_a$  and  $T_a$  are the rotation matrix and translation vector of the pose  $P_a$ , respectively.  $\omega_r$  is the weight for rotation distance, and  $s_R$  and  $s_T$  are scale factors to ensure rotation and translation distances have the same scale. We calculate the rotation distance  $D_R$  as:

$$D_R(R_a, R_b) = \arccos\left(\frac{\text{trace}(R_a R_b) - 1}{2}\right), \quad (9)$$

and the translation distance  $D_T$  as:

$$D_T(T_a, T_b) = \|T_a - T_b\|_2. \quad (10)$$

After calculating the distances of all  $P_c$  and  $\{P_i^l\}_{i=1}^L$ , we add the new pose  $P_{\text{new}}$  with minimal distance to the list:

$$P_{\text{new}} = \arg \min_{P_c \in \{P_i\}_{i=1}^K \setminus \{P_i^l\}_{i=1}^L} D_{PL}(P_{\text{new}}, \{P_i^l\}_{i=1}^L). \quad (11)$$

If  $P_{\text{new}}$  is closer to  $P_{\text{head}}^l$ , we add an edge from  $P_{\text{head}}^l$  to  $P_{\text{new}}$  and turn  $P_{\text{new}}$  into  $P_{\text{head}}^l$ ; otherwise, we do the same for  $P_{\text{tail}}^l$ . We iteratively perform this process until all poses in  $\{P_i\}_{i=1}^K$  are added to the list. After that, we start from  $P_{\text{head}}$  and traverse the whole list by edges to get an ordered set of poses  $\{P_i^l\}_{i=1}^K$  (i.e.,  $\{P_i^l\}_{i=1}^K$ ).

According to  $\{P_i^l\}_{i=1}^K$ , we obtain the ordered images  $\{I_i^l\}_{i=1}^K$ . Along the ordered poses  $P_1^l, P_2^l, \dots, P_K^l$ , we actually obtain an appropriate implicit camera trajectory. We show this process in both Alg. 2 and Fig. 10.

#### 7.2. Sampling Implicit Views

At each iteration, given  $N$  ordered poses  $\{P_i^l\}_{i=1}^N$  and corresponding  $N$  inconsistent images  $\{I_i^l\}_{i=1}^N$ , our goal now

---

#### Algorithm 1 UniVerse

---

**Input:** Inconsistent multi-view images  $\{I_i\}_{i=1}^K$ , rough camera poses  $\{P_i\}_{i=1}^K$ , camera pose estimation method  $Camera(\cdot)$  conditional video diffusion model  $\mathcal{V}(\cdot)$ , number of images per iteration  $N$ , pose sort function  $ThreadPose(\cdot)$ , the function to turn images to initial videos  $I2V(\cdot)$ , transient occlusions segment model  $Seg(\cdot)$ , 3D Reconstruction Method  $Recon(\cdot)$

```

1: Initialization:  $I^{re'l} \leftarrow \{\}$ 
    $\{I_i^l\}_{i=1}^K, \{P_i^l\}_{i=1}^K \leftarrow ThreadPose(\{I_i\}_{i=1}^K, \{P_i\}_{i=1}^K)$ 
    $I_{sty} \leftarrow$  manually/random choose an image from  $\{I_i^l\}_{i=1}^N$ 
2: while  $K > 1$  do
3:   Initiate inpainting and style masks  $M^{in} \leftarrow \{\}, M^{st} \leftarrow \{\}$ 
4:   Extract the first  $N$  images:  $\{I_i^l\}_{i=1}^N$ 
5:    $\mathbf{v}^{ini} \leftarrow I2V(\{I_i^l\}_{i=1}^N, f)$ ,  $\mathbf{v}^{ini}$  refers to initial video
6:   for each frame  $v_j$  in  $\mathbf{v}^{ini}$  do
7:     if  $v_j \in \{I_i^l\}_{i=1}^N$  then
8:       Mask transient occlusions:  $M_j^{in}, v_j \leftarrow Seg(v_j)$ 
9:     else
10:      Fill the inpainting mask  $M_j^{in}$  with "1"
11:    end if
12:    if  $v_j$  is  $I_{sty}$ , then
13:      Fill style mask  $M_j^{st}$  with "1".
14:    else
15:      Fill style mask  $M_j^{st}$  with "0".
16:    end if
17:     $M^{in}.append(M_j^{in}), M^{st}.append(M_j^{st})$ 
18:  end for
19:   $\mathbf{v}^{re} \leftarrow \mathcal{V}(\mathbf{v}^{ini}, M^{in}, M^{st})$ 
20:  Extract the restored images  $\{I_i^{re'l}\}_{i=1}^N$  from  $\mathbf{v}^{re}$ 
21:   $I^{re'l} \leftarrow I^{re'l} \cup \{I_i^{re'l}\}_{i=1}^N$ 
22:   $I_{sty} \leftarrow I_N^{re'l}$ 
23:   $\{I_i^l\}_{i=1}^K \leftarrow \{I_i^l\}_{i=N+1}^K, K \leftarrow \max(K - N, 0)$ 
24:   $\{I_i^l\}_{i=1}^K \leftarrow \{I_N^{re'l}\} \cup \{I_i^l\}_{i=1}^K$ 
25:  Update  $K \leftarrow K + 1$ 
26: end while
27: # now we get consistent images  $I^{re'l}$  (i.e.  $\{I_i^{re'l}\}_{i=1}^K$ )
28:  $\{P_i^l\}_{i=1}^K \leftarrow Camera(I^{re'l})$  # estimate poses again using consistent images
29: Output: the reconstructed 3D scene  $Recon(I^{re'l}, \{P_i^l\}_{i=1}^K)$ 

```

---

is to create a initial video of  $f$  frames including all the input  $N$  images. And we inflate it to  $f$  frames by sampling

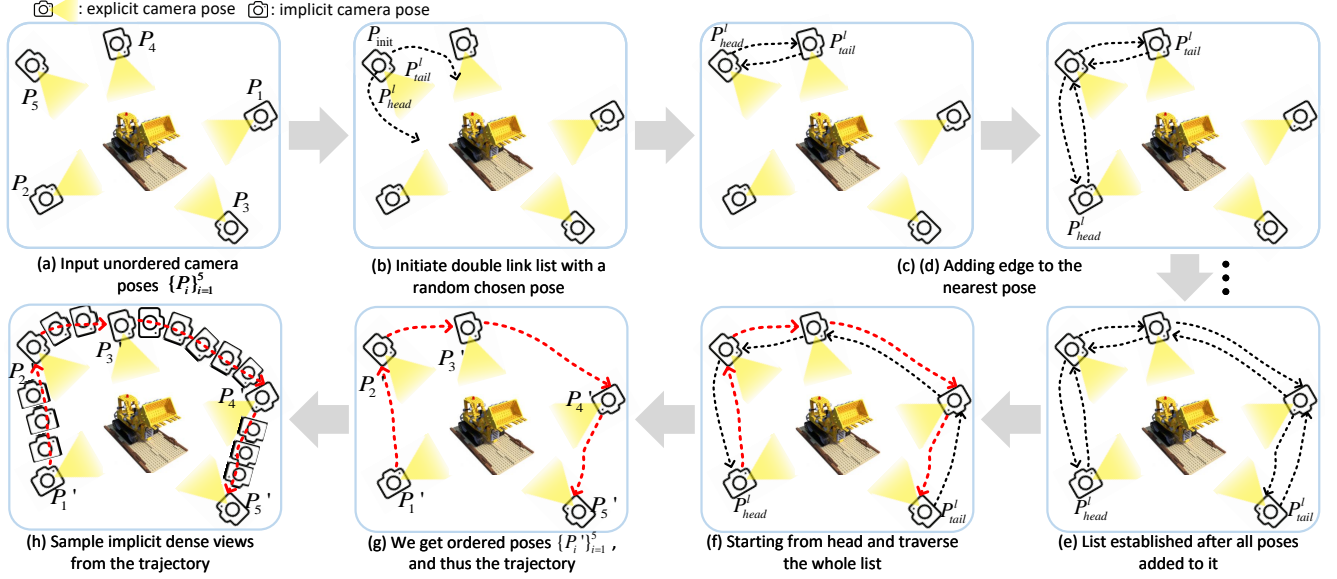


Figure 10. The flowchart of how we transform a set of multi-view images into an initial video. Here we take an example with 5 input images and their poses. Given 5 unordered poses shown in (a), we firstly random choose a pose to initiate a double link list in (b). Next, we iteratively add the nearest pose to the list until all poses are in the list, shown in (c)(d)(e). Then in (f) we start from the head of the list and traverse the whole list and obtain the ordered poses in (g). Finally we add new poses to the intervals of input poses, making the trajectory dense and thus transform images to video.

### Algorithm 2 ThreadPose for Implicit Camera Trajectory

**Input:** Poses  $\{P_i\}_{i=1}^K$ ,  $add\_edge(\cdot)$  func to add bidirectional edges,  $Traverse(\cdot)$  func to traverse the list by edges

- 1: Initialize a double linked list  $\{P_i^l\}_{i=1}^L$  with a randomly chosen pose  $P_{init} \in \{P_i\}_{i=1}^K$
- 2: Set  $L \leftarrow 1$ ,  $P_1^l \leftarrow P_{init}$
- 3: **while**  $\{P_i\}_{i=1}^K \setminus \{P_i^l\}_{i=1}^L$  **is not empty do**
- 4: Find the pose  $P_{new}$  with the minimal distance:
 
$$P_{new} = \arg \min_{P_c \in \{P_i\}_{i=1}^K \setminus \{P_i^l\}_{i=1}^L} D_{PL}(P_{new}, \{P_i^l\}_{i=1}^L)$$
- 5: **if**  $D_P(P_{new}, P_{head}^l) < D_P(P_{new}, P_{tail}^l)$  **then**
- 6:  $P_{head}^l.add\_edge(P_{new})$
- 7:  $P_{head}^l \leftarrow P_{new}$
- 8: **else**
- 9:  $P_{tail}^l.add\_edge(P_{new})$
- 10:  $P_{tail}^l \leftarrow P_{new}$
- 11: **end if**
- 12:  $L \leftarrow L + 1$
- 13: **end while**
- 14:  $\{P_i^l\}_{i=1}^K \leftarrow Traverse(P_{head}^l)$
- 15: **Output:** Ordered poses  $\{P_i^l\}_{i=1}^K$

the distances  $\{d_i\}_{i=1}^{N-1}$  between neighboring poses:

$$d_i = D_P(P_i^l, P_{i+1}^l), \quad i = 1, 2, \dots, N-1. \quad (12)$$

Next, we determine the number of new poses  $n_i$  to be inserted between each pair of neighboring poses  $P_i^l$  and  $P_{i+1}^l$ , proportional to the distance  $d_i$ :

$$n_i = \left\lfloor \frac{d_i}{\sum_{i=1}^{N-1} d_i} \times (f - N) \right\rfloor, \quad i = 1, 2, \dots, N-1, \quad (13)$$

where  $\lfloor x \rfloor$  denotes the floor function, which gives the greatest integer  $\leq x$ . Since the sum of  $n_i$  might not exactly equal  $f - N$  due to the floor operation, we distribute the remaining poses. We calculate the remaining number of poses  $r$ :

$$r = (f - N) - \sum_{i=1}^{N-1} n_i. \quad (14)$$

Then, we add one additional pose to the  $r$  largest intervals (i.e., the intervals with the largest  $d_i$  values) by incrementing  $n_i$  for the  $r$  largest  $d_i$  values:

$$n_i = n_i + \begin{cases} 1 & \text{if } d_i \text{ is among the } r \text{ largest values,} \\ 0 & \text{otherwise.} \end{cases} \quad (15)$$

In this way, we obtain the number of inserted views. By inserting  $n_i$  zero frames into neighboring images  $I_i^l, I_{i+1}^l$ , we get the initial video.

$f - N$  new poses and thus new views. First, we compute

## 8. More Implementation Details

**Adapt Video Diffusion Models with Mask Input:** We fine-tune the Video Diffusion Model from the  $576 \times 1024$  interpolation model of ViewCrafter [67]. Since our method utilizes additional masks (*i.e.* inpainting masks and style masks), we need to change the input dimension of the Denoising U-Net. We follow the fine-tuning approach of Inpainting Latent Diffusion [37]. Specifically, we change an  $8 \times C \times kernel\_size \times kernel\_size$  2D convolutional kernel to  $10 \times C \times kernel\_size \times kernel\_size$  by concatenating two additional masks. To do this, we maintain the original  $8 \times C \times kernel\_size \times kernel\_size$  kernels and add zero-initialized  $2 \times C \times kernel\_size \times kernel\_size$  kernels to it.

**Detect All Transient Objects in Input Images:** In the UniVerse pipeline, it is important to identify all transient objects to mask them. To achieve this, we first pre-define a set of transient prompts, such as [person, car, bike]. We then use a Semantic Segmentation Model to detect the pixels of the objects in the prompts. Using the positions of these pixels, we employ the Segment Anything Model (SAM) [24] to precisely segment the objects and obtain the inpainting masks.

## 9. More Visual Results

Since UniVerse utilizes a VDM to turn initial videos into restored videos, we present several examples in Figs. 11, 12, and 13, demonstrating how UniVerse leverages the video prior to transform multi-view images into a consistent video. In these figures, the top row shows the initial video frames, while the bottom row displays the corresponding restored video frames. The frames are arranged from left to right in sequential order, with the first row showing frames 1-5, the second row showing frames 6-10, and so on.

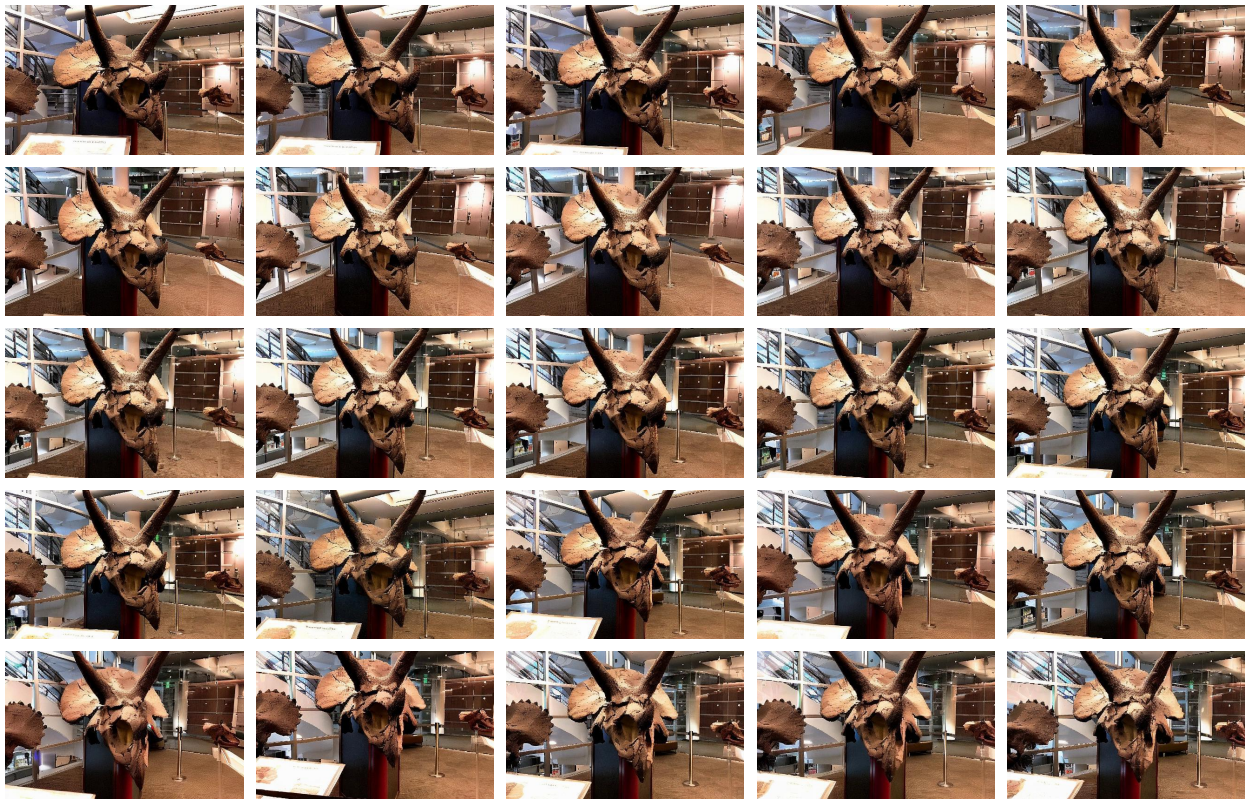
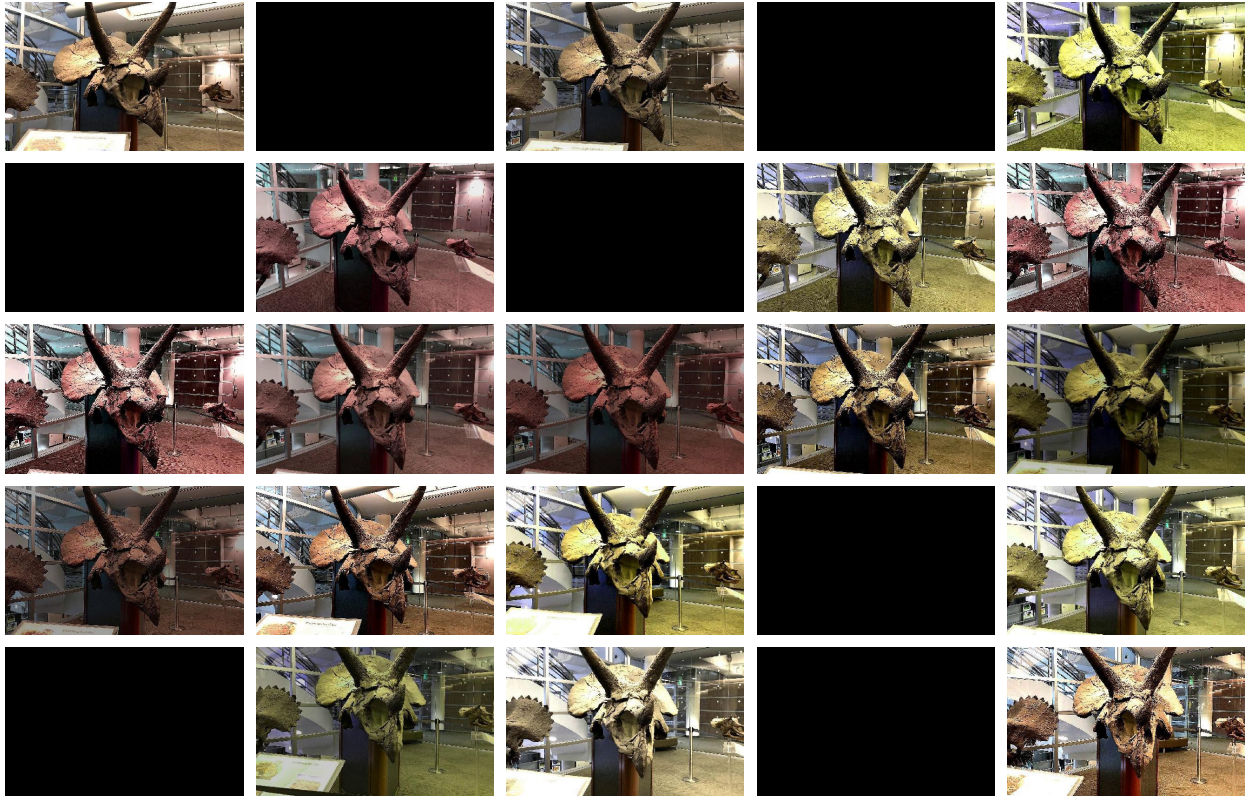


Figure 11. Visualization of how UniVerse turns a initial video into restored video.

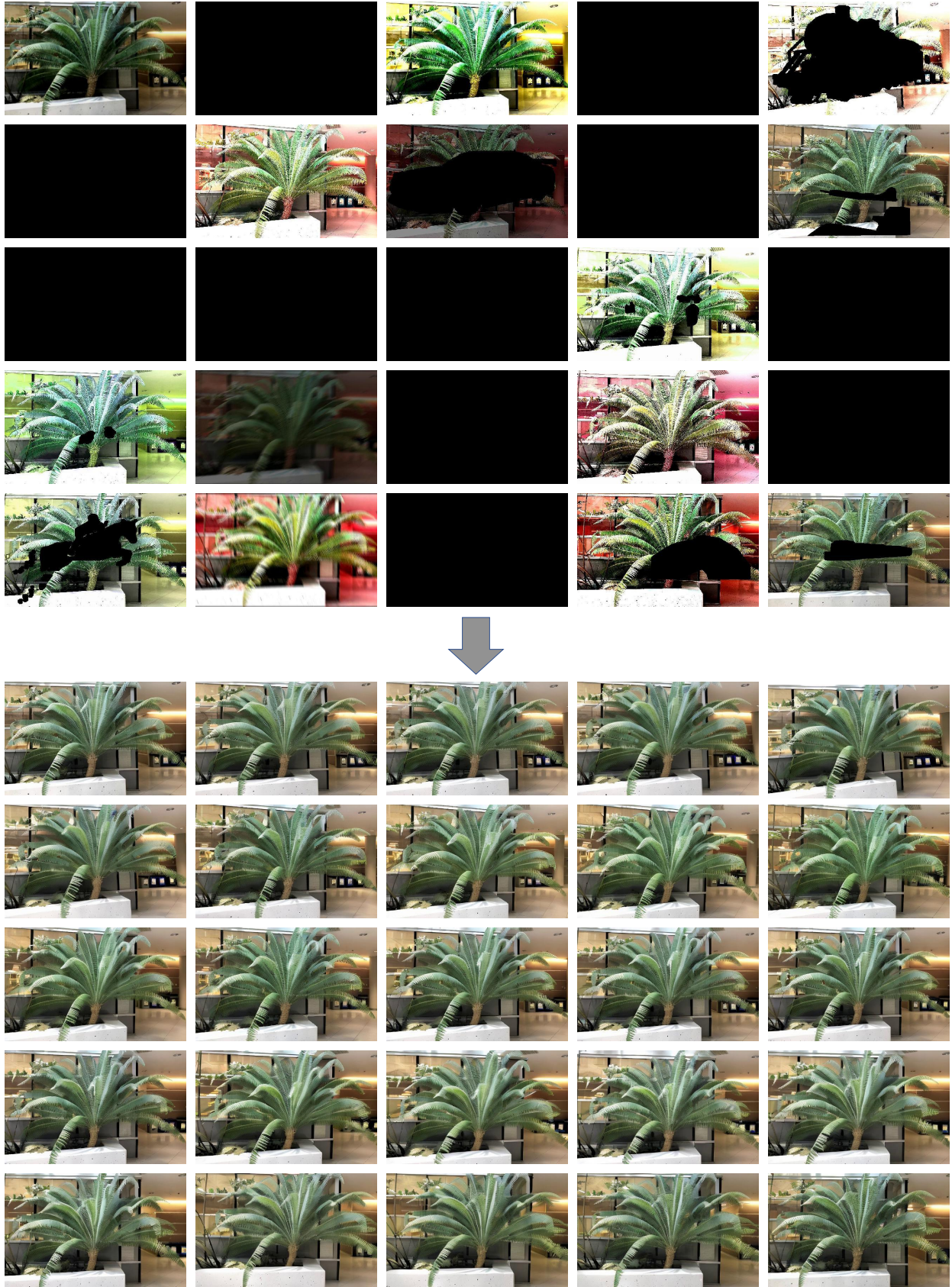


Figure 12. Visualization of how UniVerse turns a initial video into restored video.

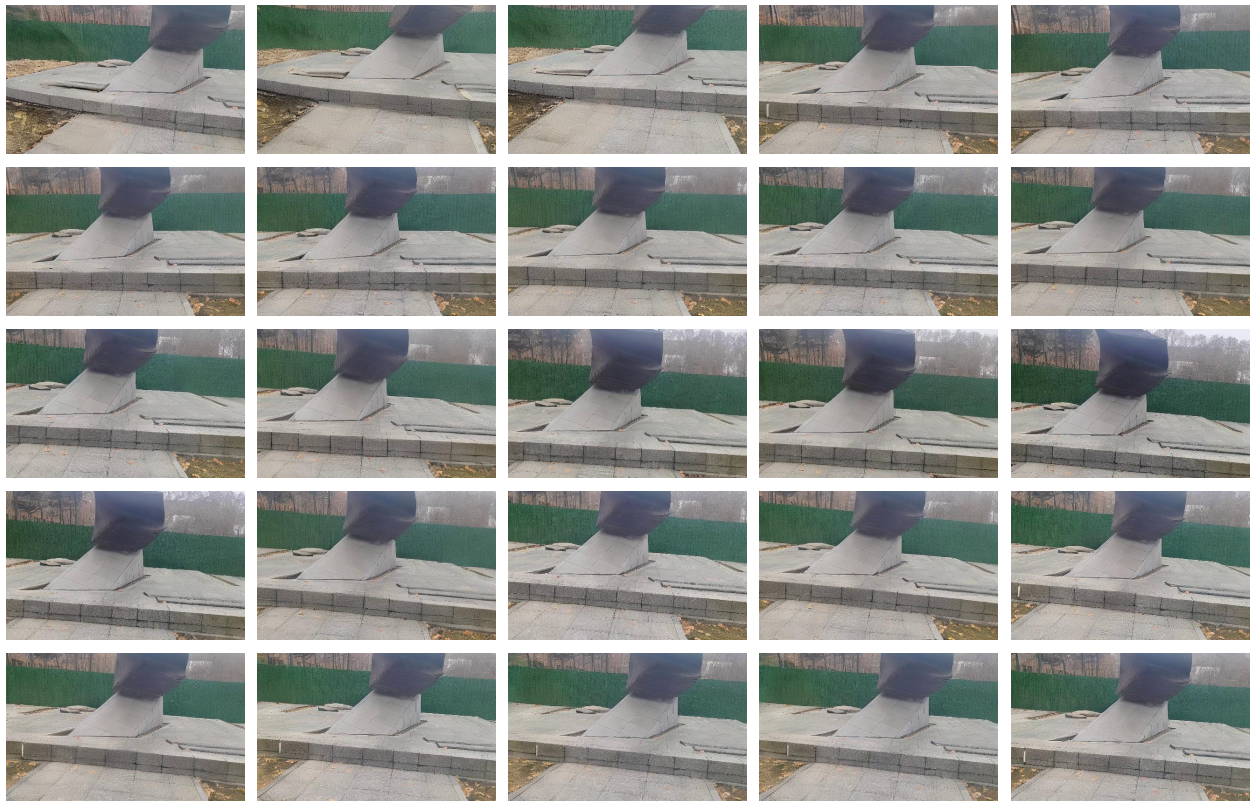
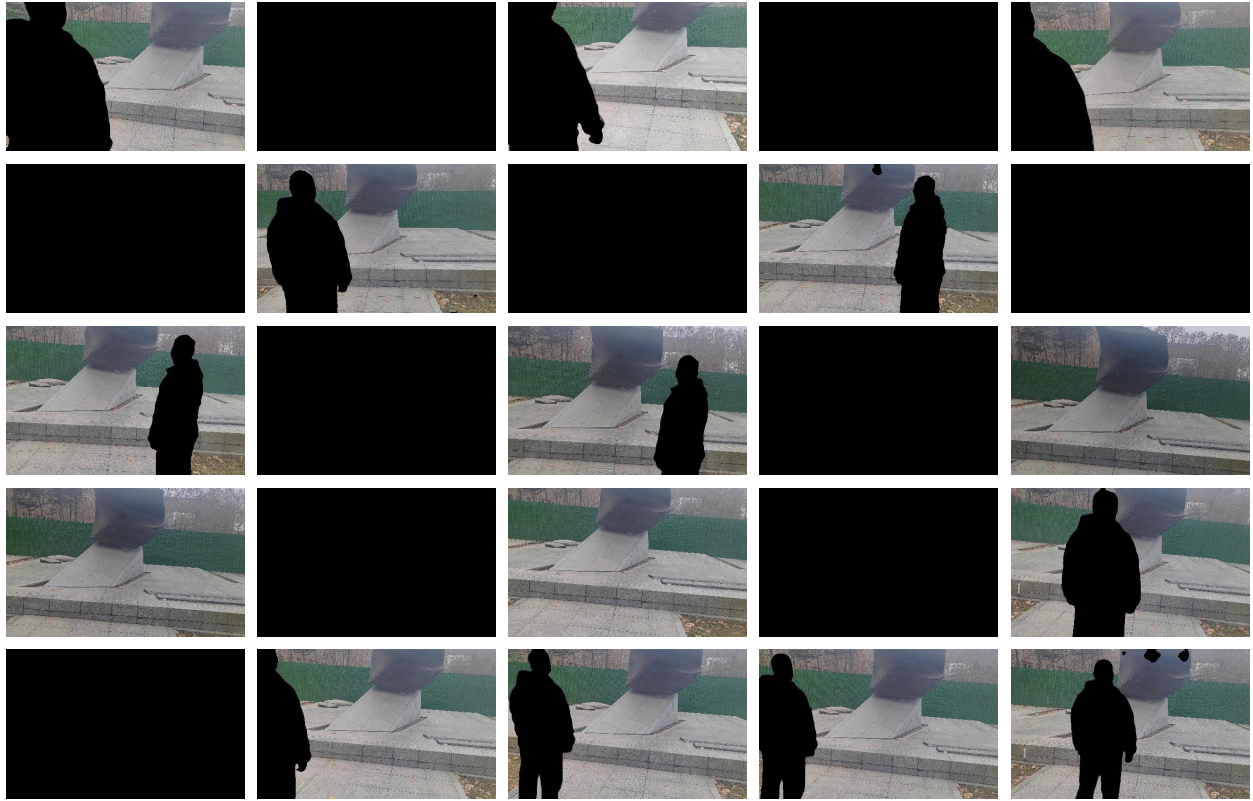


Figure 13. Visualization of how UniVerse turns a initial video into restored video.